

Cite this article as: Ma Xuyi, Duan Ai Qin, Lu Wei, et al. Influence of Heat Input on Welding Processes, Weld Formation, Microstructure, and Mechanical Properties of Double-Sided Laser Beam Welded Ti-6Al-4V Alloy T-Joints[J]. Rare Metal Materials and Engineering, 2021, 50(07): 2300-2307.

ARTICLE

Influence of Heat Input on Welding Processes, Weld Formation, Microstructure, and Mechanical Properties of Double-Sided Laser Beam Welded Ti-6Al-4V Alloy T-Joints

Ma Xuyi, Duan Ai Qin, Lu Wei, Wang Xuedong

Science and Technology on Power Beam Processes Laboratory, AVIC Manufacturing Technology Institute, Beijing 100024, China

Abstract: The Ti-6Al-4V alloy T-joints were prepared by double-sided synchronized laser beam welding with homologous filler wires. Influence of heat input on the stability of welding process, weld formation, microstructure, and mechanical properties of Ti-6Al-4V alloy T-joints was investigated through the high-speed camera during double-sided laser beam welding process. Results show that the heat input has a significant effect on molten pool behavior and droplet transition, which influences the appearance and welded quality of the T-joints. With the increase of heat input, the morphologies of welded T-joints change and the grain size increases. Martensite forms at the heat affected zone (HAZ) and fusion zone (FZ), resulting in the fact that the microhardness of HAZ and FZ is higher than that of the skin. Moreover, the tensile strength of welded T-joints along the directions of skin and stringer increases with increasing the welding heat input. The fractures occur at the base metal part of all the specimens, which is correlated with the martensitic strengthening effect of the joints.

Key words: Ti-6Al-4V alloy; double-sided laser beam welded T-joint; high-speed photography; microstructure; mechanical property; infrared thermography

In order to improve the intensity and rigidity of thin-walled structures, the stiffeners are generally employed, which have been widely used in the fields of aviation and astronautics due to their low mass. Till now, the join of stiffeners to thin-walled structures is conducted by riveting and resistance spot welding. However, by virtue of the increasingly strict requirements of low mass, high reliability, and long life, these methods have some shortcomings, such as low production rate, high structure mass, and high cost, as reported by Schubert et al^[1]. In order to tackle these problems, laser beam welding processing is gradually applied because of its high producing speed, low distortions, and lightweight, compared with the traditional methods, according to the research of Fournier^[2]. As reported by Chen et al^[3], the double-sided laser beam welding has been used to manufacture T-joints of aluminum fuselage panels for Airbus A380 and C919 in China.

Many researches have been conducted to prepare T-type structures by laser beam welding. Yang et al^[4] pointed out that

the morphology and the mechanical properties of the welded aluminum alloy T-joints are closely correlated with the welding parameters such as incident beam position, beam angle, and beam separation distance. According to Li et al^[5], the welding parameters, such as welding speed and laser power, have significant effect on the mechanical properties of laser beam welded aluminum T-joints. Oliveira et al^[6] optimized the welding parameters including shielding gas, seam angle, beam focal position, and beam position of one-sided laser beam welding for the manufacture of aluminum alloy T-joints. Squillace et al^[7] concluded that the mechanical properties of aluminum alloy welded T-joints are dependent on the composition of filler wire, and the strengthening of heat affected zone (HAZ) is attributed to the usage of high melting latent heat filler wire. Tao et al^[8] investigated the effect of the wire feeding posture for welding process, and believed that it strongly influences the wire melting behavior, process stability, and porosity defects. Most of these studies focused

Received date: July 09, 2020

Foundation item: Defense Industrial Technology Development Program (JCKY2016205A001)

Corresponding author: Ma Xuyi, Ph. D., Senior Engineer, Science and Technology on Power Beam Processes Laboratory, AVIC Manufacturing Technology Institute, Beijing 100024, P. R. China, Tel: 0086-10-85701494-801, E-mail: 15810466106@163.com

Copyright © 2021, Northwest Institute for Nonferrous Metal Research. Published by Science Press. All rights reserved.

on the manufacture of aluminum alloy T-joints. Due to the difference in physical characteristics, the double-sided laser beam welding process of titanium alloy is quite different from that of aluminum alloy in the perspective of welding equipment, the selection of welding parameters, and the mechanism of defect formation.

In the present research, the double-sided synchronized laser beam welding was employed to join titanium T-type joints with the homologous filler wire, and influences of laser heat input on the weld formation and mechanical properties were investigated through the high-speed photography of welding process and microstructural and mechanical analyses of the joints.

1 Experiment

The stringer and the skin employed in this work were rolled sheets of Ti-6Al-4V alloy with the thickness of 1.5 and 2 mm, respectively. The homologous filler wires with the diameter of 1.0 mm were used. The chemical composition of the Ti-6Al-4V alloy is listed in Table 1. In order to remove the oil and oxide film, the surfaces of sheets and filler wires were welded by degreasing and pickling. Then, the weld surfaces were ground with scratch brush and swabbed with ethanol.

The T-joints were fabricated by double-sided synchronized laser beam welding system with different heat inputs (28, 21, 16.8, and 14 J/mm), as shown in Fig. 1. Two TRUMPF Nd-YAG laser beams of 3 kW were symmetrically located at both sides of the stringer. The focus length was 200 mm, and the spot was 0.6 mm in diameter. The robot system was used to ensure the synchronism of the laser beams during the welding process. The ultrahigh purity argon gas (99.999%) was used as the shielding gas in this research, which was coaxially delivered with the laser beam and sprayed from the shielding coat. The filler wire was fixed on the same plane and fed into the molten pool along the leading direction. The laser incident

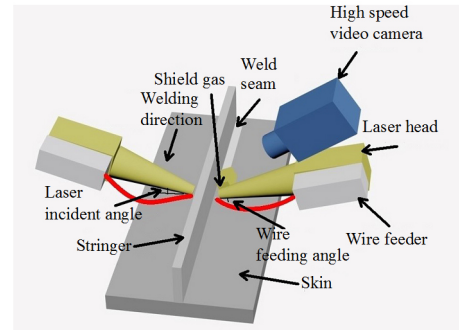


Fig.1 Schematic diagram of double-sided synchronized laser beam welding system

angle to the skin and the wire feeding angle to the laser beam were obtained according to the pre-experiment for the stable weld formation. A mega high-speed B/W & Color CMOS camera was fixed on the worktable to record the characteristic of molten pool, filler wire, and plasma/metal vapor during the welding process. The parameters used in this research are listed in Table 2.

The cross sectional appearance of weld and morphologies of welded joints were observed by a Leica DM6000M optical microscope (OM). The sizes of the molten pools and the weld beads were measured by the video screenshots obtained under different welding conditions using the commercial Image-Pro Plus (IPP) software.

The microhardness of the welded T-joints was measured by a SOI HXD1000 hardness tester at room temperature with the test load of 1.96 N and a dwell time of 15 s. The measurement was fixed across the center line of T-joints with an interval of 0.2 mm. As shown in Fig.2 and 3, two types of tensile specimens were welded referring to GB/T228-2002 to evaluate the tensile properties of the T-joints along the skin and stringer directions. The clamping device was designed to conduct the tensile test along the stringer direction. A Zwick Roell Z100 tensile tester was used to perform the tensile tests with a displacement rate of 2 mm/min at room temperature. Three specimens under the same condition were tested in this

Table 1 Chemical composition of Ti-6Al-4V alloy (wt%)

Al	V	Fe	C	N	H	O	Ti
5.5~6.8	3.5~4.5	<0.3	<0.03	<0.02	<0.01	<0.2	Bal.

Table 2 Related parameters of welding system

System	Parameter	Value
Welding process	Laser power/W	2800
	Welding speed/m·min ⁻¹	6~12
	Wire feed rate/ m·min ⁻¹	2
	Laser incident angle/(°)	30
	Wire feeding angle/(°)	35
	Shielding gas flow rate in coaxial/L·min ⁻¹	25
	Shielding gas flow rate in back/L·min ⁻¹	15
High-speed video camera	Resolution	1280×500
	Frame frequency/frames per second (FPS)	2000
Infrared thermography camera	Resolution	640×512
	Frame frequency/FPS	115

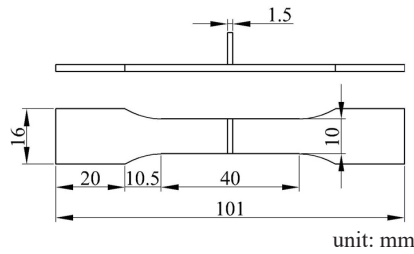


Fig.2 Schematic diagram of tensile specimen along skin direction

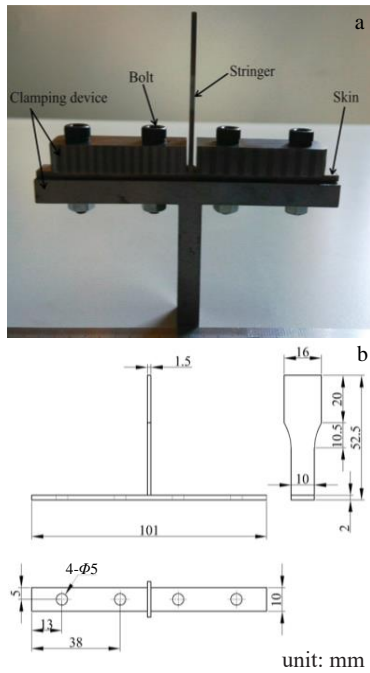


Fig.3 Clamping device (a) and schematic diagram of tensile specimen along stringer direction (b)

research. The process of tensile test was recorded by FLIR SC7000 infrared thermography camera, and the related

parameters of camera are listed in Table 2.

2 Results and Discussion

2.1 Influence of heat input on welding process

The images of molten pools with different welding parameters obtained by high-speed photography are shown in Fig.4. As shown in Fig.4a, the molten pool appears in a spindle-like shape with the width of 1.5 mm and the length of 13 mm. With decreasing the heat input from 28 J/mm to 14 J/mm, the width and length of welding pool gradually narrow to 1.2 and 6 mm, respectively. The area of molten pool also reduces with the decrease of welding heat input due to the decrease of welding energy. Moreover, it can be seen that the decrease in length of molten pool is more obvious than that in width with decreasing the welding heat input, which is mostly correlated with the laser power and the welding speed.

In addition, the volume of the plasma/metal vapor gradually increases with the decrease of heat input, which is generally related to the welding penetration for the deep penetration welding of laser beam, as reported by Duan^[9]. Under the condition of the same laser power, a large amount of plasma/metal vapor enters the keyhole, which correspondingly causes the decrease of plasma/metal vapor above the molten pool. With the decrease of heat input, the welding depth of keyhole decreases, and then the volume of plasma/metal vapor entering the keyhole decreases, resulting in the increase of volume of plasma/metal vapor above the molten pool. Meanwhile, the eruption resistance of plasma/metal vapor weakens with the decrease of heat input, resulting in the increase of the volume of plasma/metal vapor.

2.2 Influence of heat input on weld formation

2.2.1 Appearance of weld seams

The appearances of weld seams with different experiment parameters are presented in Fig.5. There are no obvious surface defects, such as crack and beading defects, which indicates that good welding formation is attained by double-sided synchronized laser beam welding. It can be seen that the

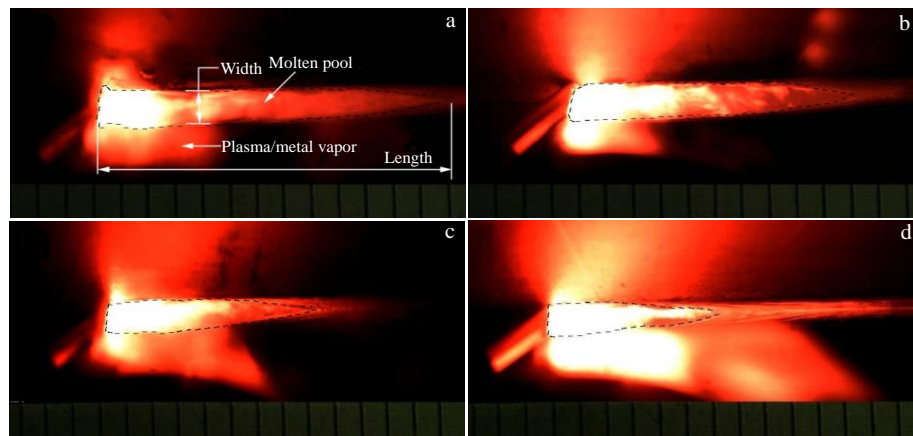


Fig.4 Images of molten pool behavior during welding process with different welding heat inputs: (a) 28 J/mm, (b) 21 J/mm, (c) 16.8 J/mm, and (d) 14 J/mm

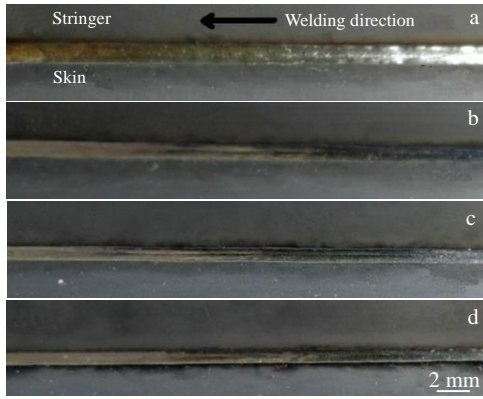


Fig.5 Weld seam appearances of T-joints with different heat inputs: (a) 28 J/mm, (b) 21 J/mm, (c) 16.8 J/mm, and (d) 14 J/mm

surfaces of the weld seams with different heat inputs are smooth. The higher the heat input, the smoother the surface of the weld seams. This phenomenon is closely related to two factors: (1) the weld flow mark is more difficult to occur during the welding of titanium alloy than that of aluminum alloy because of the lower thermal conductivity and slower cooling rate of titanium alloy; (2) the droplet between filler wire and molten pool transfers continuously under different welding heat inputs, and the smooth surface of weld seam is related to the smooth flow of molten metal at the back position of the molten pool, which is mainly caused by the decreasing temperature gradient of the molten pool along the welding direction with increasing the length of the molten pool, as shown in Fig.4.

2.2.2 Inner formation of weld seams

The cross-sectional images of welded T-joints under different welding heat inputs are shown in Fig. 6. With the decrease of welding heat input, the cross-sectional morphologies of the T-joints change obviously from the shape of circular arc to the shape without fusion defects. The weld penetration to skin, weld penetration along laser incident direction, minimum width of fusion zone (FZ), width of heat affected range, and the area of weld toe with different welding heat inputs were measured to analyze the effect of heat input on the inner formation of weld, as shown in Fig. 7. It can be seen that all these values increase with increasing the welding heat input. The lack of fusion defect appears when the welding heat input is not large enough, as indicated by the unconnected molten pools on the two sides of stringer. With the increase of the welding heat input, two molten pools connect to form a joint molten pool. The values of the weld penetration to skin increase significantly, which is attributed to the energy accumulation caused by the joint molten pool. Moreover, the size of heat affected range is dependent on the dwell time while the temperature is above the phase transition temperature during weld cooling process, which is the reason why the sizes of heat affected zone fabricated by high welding heat input are larger than that fabricated by low welding heat input. The areas of weld toes are proportional to welding heat input, which is related to the large amount of filler wire under low welding speed.

According to the research of Chen^[10], the generation of pore during the deep penetration welding with unfused joints is correlated with the welding speed. The collapse occurs at the bottom of keyhole due to the high heat input under low welding speed, and then the enclosure space (pore) is

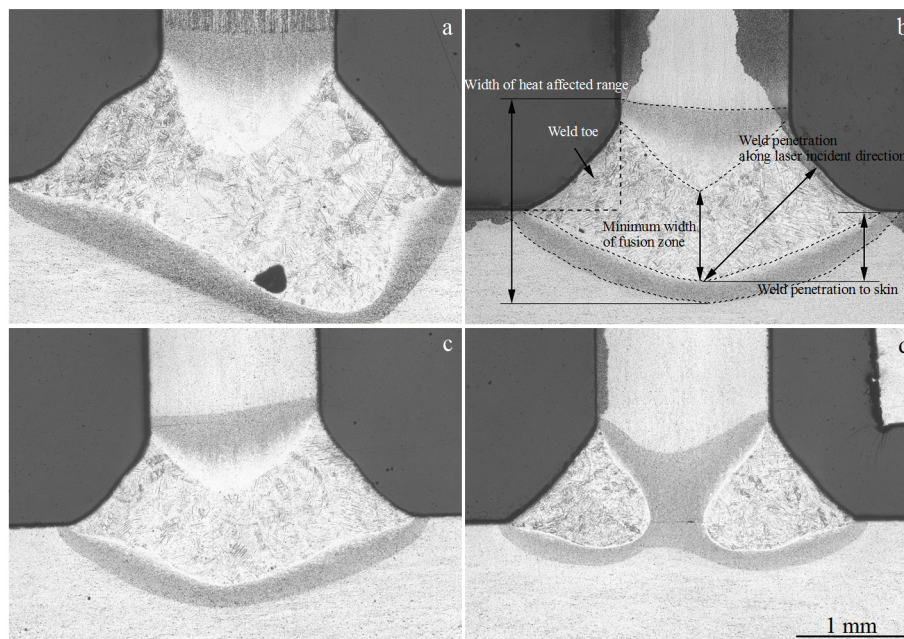


Fig.6 Cross-sectional images of welded T-joints with different welding heat inputs: (a) 28 J/mm, (b) 21 J/mm, (c) 16.8 J/mm, and (d) 14 J/mm

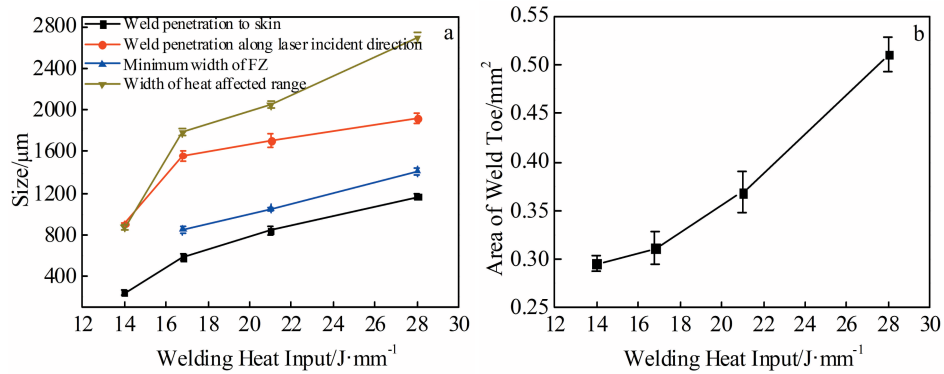


Fig.7 Size distribution (a) and weld toe area (b) of welded T-joints under different welding heat inputs

separated from the keyhole. Moreover, the larger welding heat input with lower welding speed leads to the increase of welding penetration. The pore is difficult to avoid because of the long distance caused by the increasing welding penetration. So the pore is easier to generate at this time.

2.3 Influence of heat input on microstructure

The welded T-joints consist of three zones: base metal (BM), HAZ, and FZ. The HAZs are disparate on both sides of FZ, which is in the shape of inverted triangle and circular arc. As shown in Fig.8, the HAZ near BM consists of a mixture of α phase and a small number of primary β phases and acicular martensitic α' phases. The HAZ near FZ consists of transformed α and martensitic α' phases. Moreover, the FZ consists of larger acicular martensitic α' phases than HAZ does, which are distributed crossly with a basket-weave structure.

It can be seen from Fig. 9 that the grain sizes of the welded T-joints at FZ decrease gradually with the decrease of

the heat input. Kou^[11] reported that the solidification microstructure is dominated by the product of temperature gradient G and growth rate R . GR represents the cooling rate which governs the size of the solidification structure. The higher the cooling rate, the smaller the grain size. With the increase of welding speed, the growth rate of solidification microstructure improves, and the temperature gradient near the molten pool increases due to the narrow width of molten pool, as shown in Fig.4. Thus, the cooling rate GR decreases with the decrease of heat input, which gradually decreases the grain size of FZ microstructure.

2.4 Influence of heat input on mechanical properties

2.4.1 Microhardness

The measurement positions and the microhardness distributions of welded T-joints produced with different parameters are presented in Fig.10. The microhardness gradually increases with the measurement position moving from BM to HAZ across the center line, reaching the maximum value at HAZ

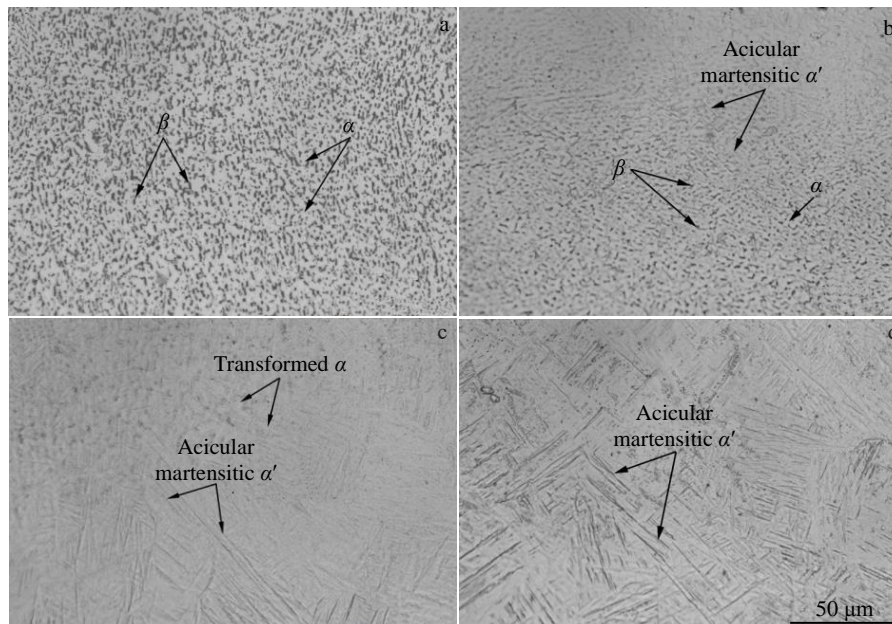


Fig.8 OM microstructures of different zones for welded T-joint: (a) BM, (b) HAZ near BM, (c) HAZ near FZ, and (d) FZ

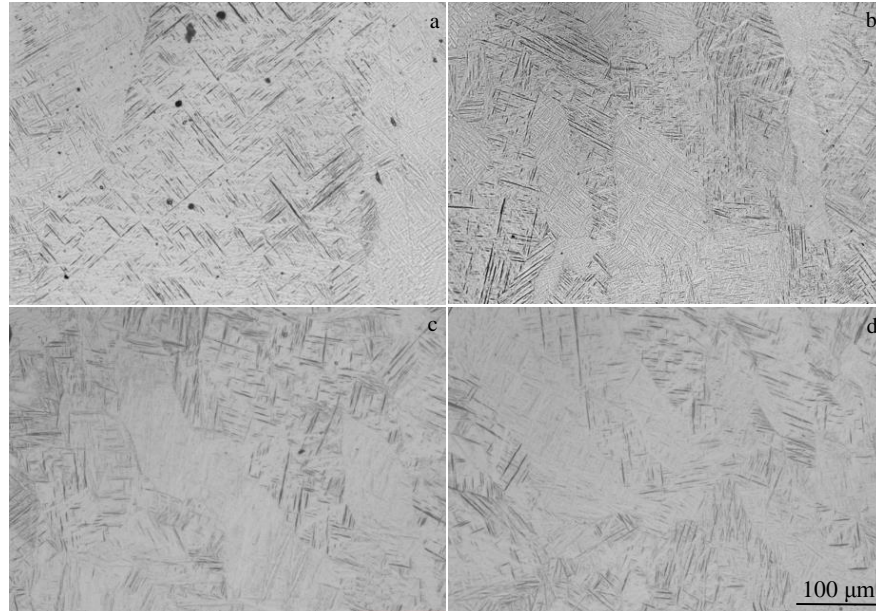


Fig.9 OM images of microstructure of FZ with different welding heat inputs: (a) 28 J/mm, (b) 21 J/mm, (c) 16.8 J/mm, and (d) 14 J/mm

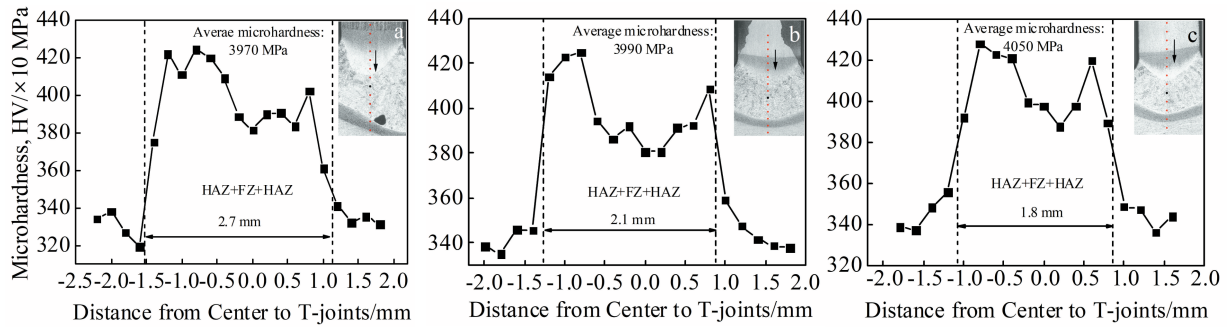


Fig.10 Microhardness distributions of welded T-joints with different welding heat inputs: (a) 28 J/mm, (b) 21 J/mm, and (c) 16.8 J/mm

near FZ. It is widely considered that the hardness strengthening in the HAZ and FZ is attributed to the formation of martensite, as reported by Lu et al^[12]. Moreover, the microhardness of HAZ is higher than that of FZ, which is correlated with the finer martensite in the HAZ compared with that in FZ. In addition, the average microhardness of HAZ and FZ decreases with increasing the welding heat input, which can be explained by the increase of martensite size with the increase of welding heat input^[11]. However, the zone with high microhardness in the T-joints reduces with the decrease of heat input, because the sizes of FZ and HAZ decrease with the decrease of heat input.

2.4.2 Tensile strength

The tensile strength of BM and the T-joints along the skin and stringer directions with different welding heat inputs is shown in Fig. 11. The tensile strength of the T-joints along the skin direction is basically equivalent to that at BM, while the tensile strength of the T-joints along the stringer direction is slightly higher than that at BM. The fractures of the tensile

specimens of the welded T-joints along the skin and stringer directions are located at BM, as shown in Fig. 12. It can be seen that the tensile strengths along both directions for welded T-joints increase with the increase of heat input. The main reason is that the weld penetration increases which leads to the improvement of strengthening area of martensite α' phase. Moreover, the tensile strength along the stringer direction is higher than that along the skin direction, which is mostly attributed to weld toes consisting of martensite α' phase. When the tensile direction is along the stringer direction, both sides of the weld toes and the strengthening area of the skin play significant roles in bearing the tensile load, whereas only the strengthening area of skin and one side of weld toes bear the tensile load when the tensile direction is along the skin direction. Thus, the tensile specimen along the stringer direction bears larger load before fracturing than that along the skin direction does, resulting in the fact that the tensile strength along the stringer direction is larger than that along the skin direction.

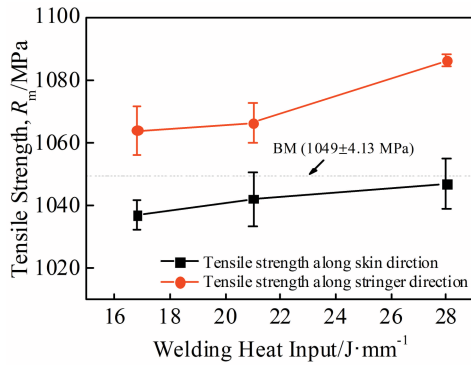


Fig.11 Tensile strength of T-joints along skin and stringer directions under different welding heat inputs

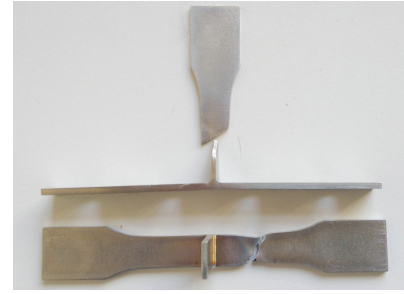


Fig.12 Appearance of tensile fractures along stringer and skin directions

The infrared thermography images of the welded T-joints during the tensile test at the plastic deformation stage are

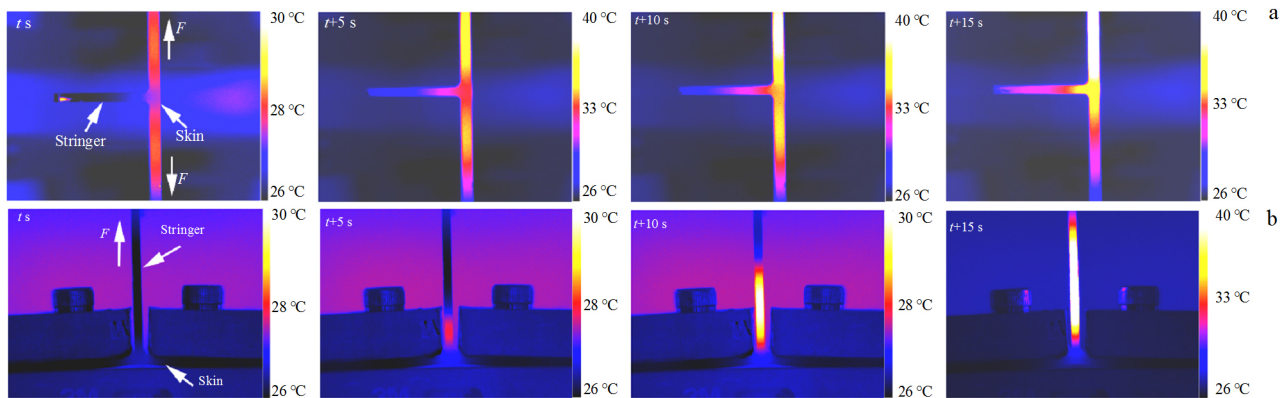


Fig.13 Infrared thermography images of welded T-joints at plastic deformation stage along skin (a) and stringer (b) directions

shown in Fig. 13. As reported by Steinberger et al.^[13], the temperature change can be used to identify the plastic deformation of materials, because the plastic deformation leads to the temperature rise of materials. It can be seen from Fig.13a that the temperature change near the welded T-joint including the weld seam and the weld toe is much less than that at BM during the tensile test along the skin direction. So the plastic deformation occurs at BM. The temperature of BM with plastic deformation increases gradually with the increase of the tension F , and the specimen finally breaks at BM with the maximum temperature. In addition, the similar process can be seen at the plastic deformation stage during the tensile test along the stringer direction, as shown in Fig.13b. These results are closely related to the formation of martensite in the welded T-joint, where HAZ and FZ are strengthened by the martensite compared with BM, and the weld toes consisting of FZ increase the strengthening area of T-joints. Therefore, the plastic deformations and fractures occur at BM of the specimens.

3 Conclusions

1) High-speed photography shows that the molten pool

appears in a spindle-like shape during the double-sided synchronized laser beam welding. The width and length of the molten pool decrease, while the volume of the plasma/metal vapor increases gradually with the decrease of the heat input.

2) Weld seams with smooth surface are obtained without obvious defects, such as crack and beading defects. With reducing the welding heat input, the width of weld seam and the size of the welded T-joints decrease, while the inner defects such as lack of fusion is observed. Moreover, the welded T-joints consist of martensitic α' phases, and the grain sizes decrease gradually with the decrease of welding heat input.

3) The microhardness gradually increases from the base metal (BM) to heat affected zone (HAZ) across the center line, reaching the maximum value at HAZ near the fusion zone (FZ) on the stringer. With increasing the heat input, the average microhardness of HAZ and FZ decreases, but the areas with high microhardness in the T-joints expand.

4) The tensile strength of welded T-joints along the skin direction is basically equivalent to that of BM, while the tensile strength of the T-joints along stringer direction is slightly higher than that of BM. The tensile strength along the

stringer direction is higher than that along skin direction, and both of them increase with the increase of heat input due to the increase of strengthening area of martensite α' phase. Moreover, the plastic deformations and fractures occur at BM of the specimens.

References

- Schubert E, Klassen M, Zerner I et al. *Journal of Materials Processing Technology*[J], 2001, 115(1): 2
- Fournier P. *Aluminium International Today*[J], 2005, 6(17): 16
- Chen Yanbin, Li Liqun, Tao Wang et al. *Laser and Tera-Hertz Science and Technology*[C]. Wuhan: OSA Laser and Tera-Hertz Science and Technology, 2012
- Yang Z B, Tao W, Li L Q et al. *Material Design*[J], 2012, 33: 652
- Li M, Li Z G, Zhao Y et al. *Advances in Materials Science and Engineering*[J], 2011, 767: 260
- Oliveira A C, Siqueira R H M, Riva R et al. *Material Design*[J], 2015, 65: 726
- Squillace A, Prisco U. *Proceedings of the Institution of Mechanical Engineers Part L: Journal of Materials, Design and Applications*[J], 2009, 223(3): 103
- Tao W, Yang Z B, Chen Y B et al. *Optics & Laser Technology*[J], 2013, 52: 1
- Duan A, Chen L. *28th International Congress on Laser Materials Processing, Laser Microprocessing and Nanomanufacturing*[C]. Orlando: ICALEO, 2009: 329
- Chen Wuzhu. *Quality Control of Laser Welding and Cutting*[M]. Beijing: China Machine Press, 2010: 65 (in Chinese)
- Kou S. *Welding Metallurgy*[M]. Hoboken: John Wiley & Sons, 2002: 174
- Lu W, Shi Y W, Lei Y P et al. *Material Design*[J], 2012, 34: 509
- Steinberger R, Leitao T, Ladstatter E et al. *International Journal of Fatigue*[J], 2006, 28(10): 1340

热输入对双光束激光焊接Ti-6Al-4V合金T型接头焊接过程、焊缝成形、组织及力学性能的影响

马旭颐, 段爱琴, 芦伟, 王学东

(中国航空制造技术研究院 高能束流加工技术重点实验室, 北京 100024)

摘要: 采用双光束同步激光填丝焊接的方法制备了Ti-6Al-4V合金T型接头, 使用高速摄像机拍摄了焊接过程图像并研究了热输入对焊接过程稳定性、焊缝成形、组织及力学性能的影响。试验结果表明, 热输入显著影响熔池行为和填丝焊接熔滴过渡, 进而影响T型接头焊缝形貌及质量。随着热输入的增加, T型接头组织发生变化, 晶粒尺寸变大。热影响区及焊缝处的马氏体使得这2个区域的显微硬度高于母材。另外, 沿蒙皮方向及筋条方向的抗拉伸强度随着热输入的增加而增大。由于接头处马氏体增强作用, 拉伸断裂均发生于母材处。

关键词: Ti-6Al-4V合金; 双光束激光焊接T型接头; 高速摄像; 组织; 力学性能; 红外热像

作者简介: 马旭颐, 男, 1983年生, 博士, 高级工程师, 中国航空制造技术研究院高能束流加工技术重点实验室, 北京 100024, 电话: 010-85701494-801, E-mail: 15810466106@163.com